International Journal of Heat and Mass Transfer 52 (2009) 2243–2254

Contents lists available at ScienceDirect

International Journal of Heat and Mass Transfer

journal homepage: www.elsevier.com/locate/ijhmt

Analysis of the turbulence–radiation interactions for large eddy simulations of turbulent flows

Maxime Roger, Carlos B. Da Silva, Pedro J. Coelho *

Mechanical Engineering Department, Instituto Superior Técnico/IDMEC, Technical University of Lisbon, Av. Rovisco Pais, 1049-001 Lisboa, Portugal

ARTICLE INFO

Article history:
Received 25 August 2008
Received in revised form 5 December 2008
Available online 4 February 2009

Keywords:
Turbulence–radiation interaction
Large eddy simulation (LES)
Radiative transfer
Direct numerical simulation (DNS)
Homogeneous isotropic turbulence

ABSTRACT

In large eddy simulations (LES) of radiative heat transfer, the subgrid-scale (SGS) radiative emission and the SGS radiative absorption are two unclosed terms that arise after applying the filtering operation to the radiative transfer equation and which represent the effect of the SGS motions on the evolution of the resolved radiative heat flux. In the present work, *a-priori* tests based on direct numerical simulation of homogeneous isotropic turbulence have been carried out. It was found that the effect of the SGS radiative absorption may be neglected in LES, whereas the SGS radiative emission has to be modelled, particularly for engineering applications where the grids are generally coarse, and in flows with high turbulence intensities. Future works should be devoted to the development of SGS models for radiative transfer.

1. Introduction

The numerical simulation of turbulent flows is an important tool in the study of many engineering and natural flows such as the ones encountered in aerodynamics, turbomachinery, combustion, oceanography or astrophysics. Direct and large eddy simulations (DNS/LES) are the most advanced and accurate numerical techniques used for modelling these flows [1]. In DNS, all the relevant scales of motion are solved, from the integral scale down to the Kolmogorov micro-scale, whereas in LES, the large energetic scales of motion are explicitly computed and the effect of the subgrid-scales (SGS) on the resolved scales is modelled. Although being virtually unmatched by any other technique, DNS is not always feasible due to its high computational cost at high Reynolds numbers, while LES can be used to compute high Reynolds number flows at reasonable cost.

LES is fast becoming a realistic alternative to the classical simulations of reactive flows using unsteady Reynolds-averaged Navier–Stokes equations (URANS) [2]. LES of turbulent combustion are particularly challenging since the chemical reactions that govern the evolution of the species concentration take place at scales of motion which are substantially smaller than the scales resolved by the LES grid [3]. However, this difficult problem has been addressed by numerous works in recent years and today it is possible to perform LES involving turbulent combustion in devices as complex as a complete gas turbine combustor [4,5].

On the other hand, much less attention has been paid to radiative transfer when LES is employed to model the flow field [6], although it is well known that radiative transfer plays an important role in many combustion systems such as boilers, furnaces, internal combustion engines and rockets. The interactions between turbulence and radiation (TRI) have been studied both theoretically and experimentally [7] and various numerical works on TRI have been developed over the last years, using RANS [8–10], PDF methods [11–13], and DNS [14,15]. However, in the LES framework, very little is known about the interaction between the turbulence and radiation, *i.e.*, TRI for LES. Usually, in combustion applications of LES, these interactions are either discarded altogether, or included in the computations without considering any subgrid-scale model for radiation [16–19]. To the author's knowledge, there is no work available in the literature about TRI modelling in LES. The only exception is the recent study from Poitou et al. [20] in which two-dimensional *a-priori* tests were carried out to assess the influence of the temperature auto-correlation and the correlation between the temperature and the absorption coefficient on the radiation emission of a methane–air triple flame. In that study, simple models based on Taylor development were proposed to reconstruct these correlations in the radiative emission, and the radiative absorption was neglected.

The goal of the present paper is to study the influence of the unresolved scales, or subgrid-scales of motion, on the resolved or grid-scale radiative absorption and emission. In particular, the present investigation is directed on assessing the relevant terms in the filtered radiative source term. This is achieved through classical *a-priori* tests where the application of several filters to a DNS data bank is used to assess several of the exact quantities involved

* Corresponding author. Tel.: +351 21 841 81 94; fax: +351 21 847 55 45.
E-mail address: pedro.coelho@ist.utl.pt (P.J. Coelho).

0017-9310/$ - see front matter © 2008 Elsevier Ltd. All rights reserved.
doi:10.1016/j.ijheatmasstransfer.2008.12.004

in LES. It is expected that the present results will guide the future modelling of TRI for LES.

The present work is a continuation of the previous work by Roger et al. [21] where the filtered radiative transfer equation (RTE) to use in LES was first studied. To simplify the analysis, combustion is not considered in the present work. We use as a starting point instantaneous fields of a passive scalar from a DNS of statistically stationary (forced) homogeneous isotropic turbulence [22]. The passive scalar field is then used to define the temperature and the chemical composition of the medium, which are decoupled from the radiative transfer calculations in the present work. Using these fields as input data, the thermal radiation is calculated with a ray-tracing/correlated *k*-distribution method. Finally, by applying a box or a cut-off filter to the data, classical *a-priori* tests are performed in order to evaluate the different terms arising from the filtered RTE.

This article is organized as follows. In the next section, the filtered RTE to solve in LES of radiative heat transfer is described. The new terms associated with the SGS radiative transfer and that require modelling are identified. In Section 3, the numerical tools for turbulence and for radiation calculations are detailed, as well as the assumptions and the models involved in these calculations. In Section 4, the results are presented and discussed. Finally, the article ends with an overview of the main results and conclusions.

2. LES of thermal radiation: the filtered radiative transfer equation

In LES, any given flow variable $Q(\mathbf{r},t)$ is decomposed into a resolved or grid-scales (GS) part $\overline{Q}(\mathbf{r},t)$, and a residual or subgrid-scales (SGS) part $Q''(\mathbf{r},t)$, through a spatial low-pass filtering operation defined as [1]

$$\overline{Q}(\mathbf{r},t)=\int Q(\mathbf{x},t)\,G(\mathbf{r}-\mathbf{x})\,d\mathbf{x} \tag{1}$$

where $G(\mathbf{r})$ represents the filter function. Therefore, any given flow variable can be decomposed as

$$Q(\mathbf{r},t)=\overline{Q}(\mathbf{r},t)+Q''(\mathbf{r},t) \tag{2}$$

The Navier–Stokes equations in the case of a viscous incompressible flow may be written as

$$\frac{\partial u_i}{\partial t}+\frac{\partial(u_iu_j)}{\partial x_j}=-\frac{1}{\rho}\frac{\partial p}{\partial x_i}+\frac{1}{\rho}\frac{\partial}{\partial x_j}\left[\mu\left(\frac{\partial u_i}{\partial x_j}+\frac{\partial u_j}{\partial x_i}\right)\right] \tag{3}$$

$$\frac{\partial u_i}{\partial x_i}=0 \tag{4}$$

Applying the filter operation, one obtains the filtered Navier–Stokes equations

$$\frac{\partial \bar{u}_i}{\partial t}+\frac{\partial(\bar{u}_i\bar{u}_j)}{\partial x_j}=-\frac{1}{\rho}\frac{\partial \bar{p}}{\partial x_i}+\frac{1}{\rho}\frac{\partial}{\partial x_j}\left[\mu\left(\frac{\partial \bar{u}_i}{\partial x_j}+\frac{\partial \bar{u}_j}{\partial x_i}\right)\right]-\frac{\partial \tau_{ij}}{\partial x_j} \tag{5}$$

$$\frac{\partial \bar{u}_i}{\partial x_i}=0 \tag{6}$$

where u_i and p are the velocity and pressure fields, respectively, μ is the dynamic viscosity, ρ the density and $\tau_{ij}=\overline{u_iu_j}-\bar{u}_i\bar{u}_j$ is the subgrid-scale stresses tensor, which describes the effect of the subgrid-scales on the resolved scales of motion and that has to be modelled. For instance, a subgrid-scale model frequently used for τ_{ij} is the well known Smagorinsky model [23]. In this model, the subgrid-scale stresses tensor is closed by assuming local equilibrium between the production and the viscous dissipation of subgrid-scale kinetic energy, and by using an eddy-viscosity assumption,

$$\tau_{ij}-\frac{1}{3}\delta_{ij}\tau_{kk}=-2\nu_t(\mathbf{r},t)\overline{S}_{ij} \tag{7}$$

where $\overline{S}_{ij}=\frac{1}{2}(\partial\bar{u}_i/\partial x_j+\partial\bar{u}_j/\partial x_i)$ is the resolved rate-of-strain tensor, and $\nu_t(\mathbf{r},t)$ is the turbulent eddy-viscosity which is modelled as $\nu_t(\mathbf{r},t)=(C_S\Delta)^2|\overline{S}|$. C_S is the Smagorinsky model constant and $|\overline{S}|=(2\overline{S}_{ij}\overline{S}_{ij})^{1/2}$ is the norm of the resolved rate-of-strain tensor. In isotropic turbulence the constant C_S is related to the Kolmogorov constant C_K through

$$C_S=\frac{1}{\pi}\left(\frac{2}{3C_k}\right)^{3/4} \tag{8}$$

Using $C_K=1.4$, we get $C_S=0.18$.

Similarly, in LES of non-isothermal flows, in addition to the filtered Navier–Stokes equations, a filtered temperature transport equation has to be solved,

$$\rho c_p\left(\frac{\partial\overline{T}}{\partial t}+\frac{\partial(\bar{u}_j\overline{T})}{\partial x_j}\right)=\frac{\partial}{\partial x_j}\left[\lambda\frac{\partial\overline{T}}{\partial x_j}\right]-\rho c_p\frac{\partial F_j}{\partial x_j}-\overline{\nabla\cdot\mathbf{q}} \tag{9}$$

where $\overline{T}$ is the resolved temperature field, λ is the thermal conductivity, c_p is the specific heat capacity and $F_j=\overline{Tu_j}-\overline{T}\bar{u}_j$ are the SGS heat fluxes requiring modelling. When present, the effects of thermal radiation arise as an additional radiative source term $\nabla\cdot\mathbf{q}$ given by [24]

$$\nabla\cdot\mathbf{q}=\int_0^{+\infty}\kappa_\nu(4\pi I_{b\nu}-G_\nu)\,d\nu \tag{10}$$

where $\mathbf{q}$ is the radiative heat flux vector and $G_\nu=\int_{4\pi}I_\nu d\Omega$ is the spectral incident radiation, which is obtained by integrating $I_\nu(\mathbf{r},\mathbf{s})$ – the spectral radiation intensity at point $\mathbf{r}$ and direction $\mathbf{s}$ – over all directions. $I_{b\nu}(\mathbf{r})$ is the spectral blackbody radiation intensity and κ_ν the spectral absorption coefficient.

The spectral radiation intensity $I_\nu(\mathbf{r},\mathbf{s})$ is governed by the radiative transfer equation (RTE) which for an emitting–absorbing and non-scattering medium may be written as

$$\frac{dI_\nu(\mathbf{r},\mathbf{s})}{ds}=-\kappa_\nu(\mathbf{r})I_\nu(\mathbf{r},\mathbf{s})+\kappa_\nu(\mathbf{r})I_{b\nu}(\mathbf{r}) \tag{11}$$

The filtered radiative transfer equation is obtained by applying a spatial filtering operation to Eq. (11)

$$\begin{aligned}\frac{d\bar{I}_\nu}{ds}&=-\overline{\kappa_\nu I_\nu}+\overline{\kappa_\nu I_{b\nu}}\\&=-\bar{\kappa}_\nu\bar{I}_\nu-(\overline{\kappa_\nu I_\nu}-\bar{\kappa}_\nu\bar{I}_\nu)+\bar{\kappa}_\nu\bar{I}_{b\nu}+(\overline{\kappa_\nu I_{b\nu}}-\bar{\kappa}_\nu\bar{I}_{b\nu})\end{aligned} \tag{12}$$

where the position $\mathbf{r}$ and the spatial direction $\mathbf{s}$ were omitted for simplicity. The terms $(\overline{\kappa_\nu I_\nu}-\bar{\kappa}_\nu\bar{I}_\nu)$ and $(\overline{\kappa_\nu I_{b\nu}}-\bar{\kappa}_\nu\bar{I}_{b\nu})$ are the spectral radiative SGS heat fluxes and have to be modelled in order to close Eq. (12).

In the following analysis, we have focused on radiative quantities integrated over the spectrum, like the Planck mean absorption coefficient κ_P and the incident mean absorption coefficient κ_G, which are defined as follows

$$\kappa_P=\frac{\int_0^{+\infty}\kappa_\nu I_{b\nu}d\nu}{\int_0^{+\infty}I_{b\nu}d\nu} \tag{13}$$

$$\kappa_G=\frac{\int_0^{+\infty}\kappa_\nu G_\nu d\nu}{\int_0^{+\infty}G_\nu d\nu} \tag{14}$$

It was assumed that the radiation is isotropic to be consistent with the assumption of isotropic and homogeneous turbulence, which allows us to write

$$\kappa_G=\frac{\int_0^{+\infty}\kappa_\nu G_\nu d\nu}{\int_0^{+\infty}G_\nu d\nu}\approx\frac{\int_0^{+\infty}\kappa_\nu I_\nu d\nu}{\int_0^{+\infty}I_\nu d\nu} \tag{15}$$

Notice that, in practical problems, the assumption of isotropic radiation is approximately valid for perfectly stirred reactors. Integration of Eq. (12) over the spectrum yields

$$\frac{d\bar{I}}{ds} = -\overline{\kappa_G I} + \overline{\kappa_P I_b} = -\bar{\kappa}_G\bar{I} - \left(\overline{\kappa_G I} - \bar{\kappa}_G\bar{I}\right) + \bar{\kappa}_P\bar{I}_b + \left(\overline{\kappa_P I_b} - \bar{\kappa}_P\bar{I}_b\right) \tag{16}$$

Integrating Eq. (11) over the spectrum and over all directions, the following expression of the radiative heat flux is obtained after some algebra:

$$\nabla\cdot\mathbf{q} = 4\pi\kappa_P I_b - \kappa_G G \tag{17}$$

or, in the case of isotropic radiation,

$$\nabla\cdot\mathbf{q} = 4\pi[\kappa_P I_b - \kappa_G I] \tag{18}$$

Eq. (18) is similar to Eq. (17), which does not require the assumption of isotropic radiation, and therefore it is expected that the conclusions drawn from the analysis of Eq. (18) remain valid for Eq. (17).

The filtered divergence of the radiative heat flux, which represents the additional source term to be used in LES of flows with radiation, is obtained by applying a spatial filtering operation to Eq. (18)

$$\begin{aligned}\overline{\nabla\cdot\mathbf{q}} &= 4\pi\left(\overline{\kappa_P I_b} - \overline{\kappa_G I}\right)\\ &= 4\pi\left[\bar{\kappa}_P\bar{I}_b - \bar{\kappa}_G\bar{I}\right] + 4\pi\left[\left(\overline{\kappa_P I_b} - \bar{\kappa}_P\bar{I}_b\right) - \left(\overline{\kappa_G I} - \bar{\kappa}_G\bar{I}\right)\right]\end{aligned} \tag{19}$$

In Eq. (19), the terms $\bar{\kappa}_P\bar{I}_b$ and $\bar{\kappa}_G\bar{I}$ are the resolved radiative emission and absorption, respectively, while the terms $(\overline{\kappa_P I_b} - \bar{\kappa}_P\bar{I}_b)$ and $(\overline{\kappa_G I} - \bar{\kappa}_G\bar{I})$ are the SGS radiative emission and the SGS radiative absorption, respectively, and represent the effect of the SGS radiation on the resolved radiative emission and absorption. These terms are the analogues of the SGS stresses and SGS scalar fluxes, for LES of radiative heat transfer, and have to be modelled.

The filtered RTE may be written as follows, after expansion of κ_P, κ_G, I and I_b on the right hand side of Eq. (16) as the sum of a resolved and a subgrid-scale component:

$$\begin{aligned}\frac{d\bar{I}}{ds} = &-\overline{\bar{\kappa}_G\bar{I}} - \left(\overline{\kappa_G''\bar{I}} + \overline{\bar{\kappa}_G I''} + \overline{\kappa_G'' I''}\right) + \overline{\bar{\kappa}_P\bar{I}_b}\\ &+ \left(\overline{\kappa_P''\bar{I}_b} + \overline{\bar{\kappa}_P I_b''} + \overline{\kappa_P'' I_b''}\right)\end{aligned} \tag{20}$$

Similarly, the filtered divergence of the radiative heat flux can be written as:

$$\overline{\nabla\cdot\mathbf{q}} = 4\pi\left[-\overline{\bar{\kappa}_G\bar{I}} - \left(\overline{\kappa_G''\bar{I}} + \overline{\bar{\kappa}_G I''} + \overline{\kappa_G'' I''}\right) + \overline{\bar{\kappa}_P\bar{I}_b} + \left(\overline{\kappa_P''\bar{I}_b} + \overline{\bar{\kappa}_P I_b''} + \overline{\kappa_P'' I_b''}\right)\right] \tag{21}$$

The terms $(\overline{\bar{\kappa}_P\bar{I}_b} - \bar{\kappa}_P\bar{I}_b)$ and $(\overline{\bar{\kappa}_G\bar{I}} - \bar{\kappa}_G\bar{I})$ are mathematically similar to the Leonard stresses, $(\overline{\kappa_P''\bar{I}_b} + \bar{\kappa}_P I_b'')$ and $(\overline{\kappa_G''\bar{I}} + \bar{\kappa}_G I'')$ to the SGS cross stresses, and $\overline{\kappa_P'' I_b''}$ and $\overline{\kappa_G'' I''}$ to the SGS Reynolds stress. Therefore, in this article, the terms $(\overline{\kappa_P''\bar{I}_b} + \bar{\kappa}_P I_b'')$ and $(\overline{\kappa_G''\bar{I}} + \bar{\kappa}_G I'')$ are referred to as the cross SGS radiation emission, and cross SGS radiation absorption terms, respectively, while the terms $\overline{\kappa_P'' I_b''}$ and $\overline{\kappa_G'' I''}$ are referred to as the SGS Reynolds emission and SGS Reynolds absorption.

3. Computational details

In this section, the numerical tools and the various procedures used to estimate the turbulence and radiation quantities are described. First, DNS of statistically stationary (forced) isotropic velocity and passive scalar fields are carried out as outlined in Section 3.1. The passive scalar fields from the DNS are used to generate both the temperature and the chemical composition fields as described in Section 3.2. These fields are then used as input data to the radiation code, which is based on a ray-tracing/correlated k-distribution method described in Section 3.3. Finally, *a-priori* tests are carried out with the results from this code by filtering the radiative emission $\kappa_P I_b$ and absorption $\kappa_G I$ fields using either a box or a cut-off filter, as described in Section 3.4.

3.1. Direct numerical simulation of statistically stationary (forced) homogeneous isotropic turbulence

The DNS data bank used in the present work consists in the statistically steady (forced) homogeneous isotropic turbulence data bank recently used by da Silva and Pereira [22,25]. The simulations were carried out with a standard pseudo-spectral code in which the temporal advancement is made with an explicit 3rd-order Runge–Kutta scheme. The physical domain consists in a periodic box of sides equal to 2π and using $N = 192$ collocation points in each spatial direction. The simulations were fully dealised using the 3/2 rule. Both the velocity and scalar large scales were forced in order to sustain the turbulence using the method described by Alvelius [26]. The forcing was imposed on three wave numbers concentrated on $k_p = 3$, for both the velocity and scalar fields. It is designed to inject kinetic energy and scalar variance during the simulation at a rate that balances the instantaneous viscous dissipation rate ε and the scalar dissipation rate ε_θ. Therefore, the velocity and the passive scalar fields are statistically stationary. Notice that the forcing affects only a very small wave number region associated with the larger scales of motion, *i.e.*, it does not affect the scales near the cut-off wave number associated with the filtering procedure used in LES.

Moreover, as described in Ref. [22], it was checked that both the large and the small scales of motion comply with the strong resolution requirements needed in DNS, *e.g.*, $L_{box} > 4L_{11}$, where L_{box} is the size of the computational domain and L_{11} is the integral scale of the velocity field, and $k_{max}\eta > 1.5$ and $k_{max}\eta_B > 1.5$, where k_{max} is the maximum resolved wave number and $\eta = (\nu^3/\varepsilon)^{1/4}$ and $\eta_B = Sc^{1/2}$ are the Kolmogorov and the Batchelor micro-scales, respectively, and Sc is the Schmidt number. Table 1 lists the most relevant physical and computational parameters of the simulation. The data bank used here consists in 40 instantaneous passive scalar fields corresponding to a Schmidt number equal to $Sc = 0.7$. Notice that due to the low wave number forcing these 40 passive scalar fields are statistically equivalent. For this simulation, the Reynolds number based on the Taylor scale is $Re_\lambda = u'\lambda/\nu = 95.6$, where $\lambda^2 = \langle u'^2\rangle/\langle(\partial u/\partial x)'^2\rangle$ is the Taylor micro-scale, $u' = \langle u'^2\rangle^{1/2}$ is the root-mean-square of the velocity fluctuations, and ν is the kinematic viscosity. As shown in Ref. [22], velocity and scalar spectra display a $-5/3$ range which shows the existence of an inertial range region. Therefore, this simulation is already representative of a high Reynolds number flow, in the sense that it features the most important characteristics of turbulence, such as a dissipation rate independent from the viscosity and the well known Kolmogorov–Obukhov $-5/3$ inertial scaling law of the energy and scalar variance spectra. More details on this simulation are given in Ref. [22].

3.2. Generation of temperature and species concentration fields from the DNS data bank

In order to generate the temperature and species concentration fields for the RTE computations, we use the passive scalar fields from the above DNS of isotropic turbulence. This is a good approximation, since the Prandtl number of major species in combustion

Table 1
Details of the direct numerical simulation. The Reynolds number Re_λ is based on the Taylor micro-scale. ν is the molecular viscosity, k_{max} the maximum resolved wave number, Sc the Schmidt number, L_{11} the velocity integral scale, η the Kolmogorov micro-scale and η_B the Batchelor micro-scale.

Re_λ	ν	Sc	$k_{max}\eta$	$k_{max}\eta_B$	L_{11}	η ($\times10^{-2}$)	η_B ($\times10^{-2}$)
95.6	0.006	0.7	1.8	2.1	1.24	2.8	3.3

flows is also near 0.7. However, as in classical DNS of isotropic turbulence, the DNS data bank used here is made of fluctuating velocity and passive scalar fields with zero mean value. This fact raises problems for the RTE computations, since a temperature field with zero mean makes no sense. For this reason, a procedure had to be developed in order to bridge the DNS and the RTE computations. This procedure is described here.

The present analysis is intended to be representative of the turbulence as found, *e.g.*, at the far field of a turbulent jet. At present, the direct effects from combustion in the computations are excluded, and only the turbulence characteristics from the gas phase, after the chemical reactions have been completed, are taken into account. Kinematic similarity between the two flows, *i.e.*, between the isotropic and the turbulence jet fields could be assumed to generate a turbulent velocity field from isotropic turbulence, which is representative of a jet at the far field. With this approximation, the velocity field for the jet, $u(\mathbf{r})$, could be obtained from the velocity field given from the isotropic turbulence, $u_{\mathrm{DNS}}(\mathbf{r})$, using the root-mean-square from the isotropic and jet fields $\langle u^2_{\mathrm{DNS}}(\mathbf{r})\rangle$ and $\langle u'^2(\mathbf{r})\rangle$, respectively,

$$u(\mathbf{r}) = \langle u\rangle + u_{\mathrm{DNS}}(\mathbf{r})\sqrt{\frac{\langle u'^2\rangle}{\langle u^2_{\mathrm{DNS}}\rangle}} \tag{22}$$

Similarly, for the temperature field, the instantaneous temperature field $T(\mathbf{r})$ at point $\mathbf{r}$ used in the radiation calculation is determined from the DNS passive scalar/temperature field according to [21,27]:

$$T(\mathbf{r}) = \langle T\rangle + T_{\mathrm{DNS}}(\mathbf{r})\sqrt{\frac{\langle T'^2\rangle}{\langle T'^2_{\mathrm{DNS}}\rangle}} \tag{23}$$

where $\langle T\rangle$ and $\langle T'^2\rangle$ are the mean value and the variance of the temperature prescribed for the radiation calculations, and $\langle T'^2_{\mathrm{DNS}}\rangle$ is the variance of the passive scalar/temperature field computed from the DNS. The molar fractions of the absorbing species are obtained similarly. Notice that in isotropic turbulence, the time-averages are equivalent to spatial-averages, which allows the evaluation of the mean value or variance of a given flow quantity using only one single instantaneous field.

As described above, our goal is to analyze TRI for LES downstream of the reaction zone at the far field of a turbulent jet. Therefore, three values of the "temperature turbulence intensity" $\sqrt{\langle T'^2\rangle}/\langle T\rangle$ = 10%, 20%, and 30%, which are typical of the ones found in flame jets [28], have been used. Moreover, a mean temperature of $\langle T\rangle$ = 1500 K, which is also a typical temperature found in flame jets, was used. Using these reference values, and the passive scalar/temperature fields from the DNS data, the instantaneous temperature fields for the radiative computations were calculated with the aid of Eq. (23).

However, this procedure raises some problems. For instance, negative temperatures may appear in some flow points, which is clearly unphysical. Furthermore, it was observed that the temperature exceeds the adiabatic flame temperature of the hydrocarbons usually encountered in combustion devices for some flow points. In order to overcome this shortcoming, minimum and maximum allowed temperatures were prescribed: $T_{\min}$ = 300 K, and $T_{\max}$ = 2500 K, respectively, *i.e.*, the minimum temperature of the system has been fixed to the atmospheric temperature, while the maximum temperature has been chosen to be near a typical maximum temperature for hydrocarbon flames. Whenever the temperature $T(\mathbf{r})$ given by Eq. (23) is beyond these limits, it is set equal to the nearest of these prescribed values, *e.g.*, the temperature at flow points where the local temperature $T(\mathbf{r})$ obtained from Eq. (23) is $T(\mathbf{r}) < T_{\min}$ is set to $T(\mathbf{r}) = T_{\min}$, and to $T(\mathbf{r}) = T_{\max}$ at flow points where $T(\mathbf{r}) > T_{\max}$.

Notice that this correction is satisfactory as long as the statistics of the temperature field are not significantly modified by the prescribed values, *i.e.*, as long as the correction affects only a small fraction of the total number of points from the data. This is indeed the case, and it can be checked in Table 2, which shows the mean, variance, skewness and flatness of the temperature field obtained from Eq. (23). The values determined without correction of the temperature field are compared with the corrected temperature field considering $T_{\min}$ = 300 K and $T_{\max}$ = 2500 K (as used in the present work). As can be seen, the skewness and flatness factors are not substantially affected by the limits set for $T(\mathbf{r})$, which gives confidence in the procedure used to generate $T(\mathbf{r})$.

Table 2
Statistical moments of the temperature field computed from Eq. (23). The values determined without correction of the temperature field ($T_{\min} = -\infty$, $T_{\max} = +\infty$) are compared with the corrected temperature field ($T_{\min}$ = 300 K, $T_{\max}$ = 2500 K), as used in the present work.

$\frac{\sqrt{\langle T'^2\rangle}}{\langle T\rangle}$ (%)	$T_{\min}$	$T_{\max}$	$\langle T\rangle$ (K)	$\sqrt{\langle T'^2\rangle}$ (K)	$\frac{\langle T'^3\rangle}{\langle T'^2\rangle^{3/2}}$	$\frac{\langle T'^4\rangle}{\langle T'^2\rangle^2}$
10	$-\infty$	$+\infty$	1500	150	0.155	3.15
10	300 K	2500 K	1500	150	0.155	3.15
20	$-\infty$	$+\infty$	1500	300	0.155	3.15
20	300 K	2500 K	1500	300	0.149	3.12
30	$-\infty$	$+\infty$	1500	450	0.155	3.15
30	300 K	2500 K	1497	440	0.0523	2.75

3.3. Radiative transfer calculations

The integral form of the RTE along a line of sight may be written as [24]

$$I_\nu(s) = I_\nu(0)\exp\left(-\int_0^s \kappa_\nu(s')ds'\right) + \int_0^s \kappa_\nu(s')I_{b\nu}(s') \times \exp\left(-\int_{s'}^s \kappa_\nu(s'')ds''\right)ds' \tag{24}$$

Eq. (24) has been discretized by dividing the optical path into elements and interpolating the temperature and chemical composition from the DNS data using cubic splines. The integrals in Eq. (24) are numerically estimated using Simpson's rule. The integration over the spectrum has been performed using the correlated *k*-distribution method [29]. In this method, the spectrum is divided into narrow bands such that the Planck function remains approximately constant within each band, and the absorption coefficient is reordered within every band into a smooth monotonically increasing function. The averaged radiation intensity over a band takes the following form

$$I_{\Delta\nu} = \frac{1}{\Delta\nu}\int_{\Delta\nu} I_\nu d\nu = \int_0^\infty I(k)f(k)dk = \int_0^1 I(g)dg \tag{25}$$

where $f(k)$ is the probability density function of the absorption coefficient in the considered band and $g(k)$ is the cumulative *k*-distribution function. The integral in Eq. (25) is evaluated using Gaussian quadrature, which yields the following relation for a mixture with only one participating species

$$I_{\Delta\nu_i} = \sum_{j=1}^{N_Q} \omega_j I_{\Delta\nu_i j}\Delta\nu_i \tag{26}$$

where ω_j is the quadrature weight, N_Q is the number of quadrature points and $I_{\Delta\nu_i j}$ is the radiative intensity for the *i*th band and for quadrature point *j*. The parameters needed for the correlated *k*-approximation are taken from the data of Soufiani and Taine [30]. The total radiation intensity is evaluated as $\int_0^{+\infty} I_\nu d\nu \approx \sum_{i=1}^{N_b} I_{\Delta\nu_i}$.

The radiation intensity along the boundary was assumed to be equal to zero in [27]. However, this boundary condition is not consistent with that used in DNS. Therefore, periodic boundary conditions were used in the present work to be consistent with the boundary conditions used in DNS. Periodic boundary conditions were also used for the radiation calculations in the DNS study of

Table 3
Details of the standard conditions used in the radiative transfer calculations.

T_{min}	T_{max}	<T>	$< X_{CO_2} >$	$\sqrt{< T'^2 >}$	$\sqrt{< X'^2_{CO_2} >}$	τ	$\frac{\sqrt{<T'^2>}}{<T>}$
300 K	2500 K	1500 K	0.5	300 K	0.1	10	20%

Deshmukh et al. in [15]. The periodicity was enforced by setting $I_\nu(0) = I_\nu(L)$ where L is the length of the radiation domain. Physically, the periodic boundary conditions imply that, for a given direction, the radiation intensity entering the domain is equal to the radiation intensity leaving the domain, *i.e.*, the medium is in radiative equilibrium. These conditions are present, for example, in well-stirred reactors. Another example where radiative equilibrium prevails, and therefore conditions are approximately periodic, is an optically thick medium, in which local emitted radiation is absorbed by the medium within a very short distance. The use of periodic boundary conditions in the RTE stems directly from the periodic DNS data of isotropic turbulence. It permits the definition of several important physical quantities, and especially a detailed assessment of the three-dimensional energy spectrum function, which turns out to be an important quantity for the physical analysis in LES framework. Other non-periodic flows, *e.g.*, turbulent jets, will be the subject of future work.

Although radiation from H_2O could easily be included in the calculations, only radiation from CO_2 is considered in this work in order to reduce computational requirements. Moreover, even though combustion is not taken into account in the present work, the temperature and the CO_2 molar fraction are supposed to be fully correlated, which is consistent with the laminar flamelet combustion model, often employed to model turbulent reactive flows. Due to this approximation, the passive scalar field from the DNS serves to generate both the temperature field and the CO_2 molar fraction used in the RTE computations.

The conditions assumed for the standard radiative transfer calculations are summarized in Table 3. The length L of the radiation domain is defined in order to satisfy the prescribed optical thickness of the medium τ estimated through $\tau = \kappa_P(< T >, < X_{CO_2} >)L$. Apart from being used to prescribe the size of the domain for the radiative transfer calculations, the optical thickness of the medium does not enter the computations. The physical parameters used for the DNS of homogeneous isotropic turbulence and for the RTE computations are characteristic of those encountered in many reactive flows.

In the case of homogeneous isotropic turbulence, the statistical data computed from a time series of a scalar along a single optical path parallel to a coordinate axis are identical to the statistical data calculated from all optical paths parallel to the coordinate axes at a given time, as illustrated in Fig. 1. The statistical data reported in Section 4 were obtained using all the available optical paths parallel to the coordinate axes, which are statistically indistinguishable, yielding $6 \times N^2$ optical paths, where $N = 192$ is the number of collocation points from the DNS.

3.4. Filtering procedure

The present work uses classical *a-priori* tests to assess several terms from the filtered RTE. In particular, the filtered radiative absorption and emission terms that have to be modelled in LES of radiative heat transfer will be investigated. Two filter types with several filter sizes are used in the *a-priori* tests. The first filter consists in the box or top-hat filter, which is defined by

$$G(\mathbf{x}-\mathbf{y}) = \begin{cases} 1/\Delta & \text{if} \quad |\mathbf{x}-\mathbf{y}| < \Delta/2 \\ 0 & \text{otherwise} \end{cases}$$

The spectral cut-off filter is also used. It is defined in the Fourier space as

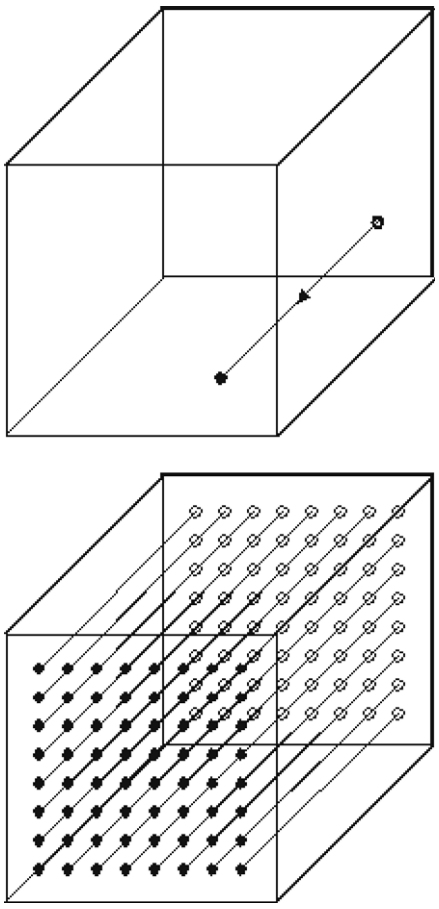

Fig. 1. Lines of sight of the radiation calculation.

$$\hat{G}(\mathbf{k}) = \begin{cases} 1 & \text{if} \quad \mathbf{k} < k_c = \pi/\Delta \\ 0 & \text{otherwise} \end{cases}$$

Notice that in the present work, the filtering operation has been applied without sampling, *i.e.*, the *a-priori* tests are done in the DNS grid.

Five different filter sizes were used with $\Delta = m\delta$, where δ is the size of the DNS grid and $m = 2$, 4, 8, 16 and 32. As shown in [22], the filter sizes $\Delta/\delta = 2$, 4 are placed in the dissipation range, while $\Delta/\delta = 8$ and 16 are representative of the inertial range region. The filter with $\Delta/\delta = 32$ is clearly in the energy-containing range. In practice, LES should be carried out using $\Delta/\delta = 8$ or 16.

In order to show the location of the filters in the radiative heat transfer quantities, Figs. 2 and 3 show the three-dimensional (spatial) spectra of the filtered emission term $\overline{\kappa_P I_b}$ obtained with the box and cut-off filters, respectively, using several filter sizes. The spectra correspond to the standard conditions (cf. Table 3).

The most important contribution for the emission term comes from the low wave number range of the spectrum. Indeed, the most important values for $\kappa_P I_b$ correspond to the wave numbers around $k = 2$ to 4. It is this important fact that makes it feasible to model this term using the LES approach, since in LES the dynamics of the low wave number range are explicitly computed, while high wave numbers, being less important, can be modelled. Moreover, notice that, as expected and in agreement with the known characteristics of these filters, the box filter affects all the wave number range, while the cut-off filter affects only wave numbers above a given cut-off wave number. Finally, notice that the effects of the filter affect the smaller wave numbers for $\Delta/\delta = 32$, *i.e.*, this filter size affects scales that should be resolved in a practical LES.

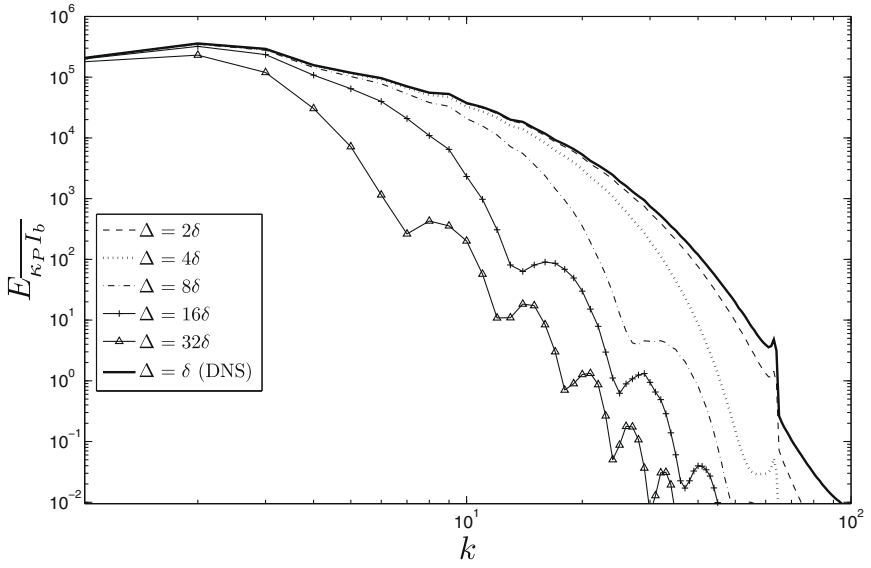

Fig. 2. Spectra of the filtered radiative emission term $\overline{\kappa_P I_b}$ for various filter sizes using the box filter.

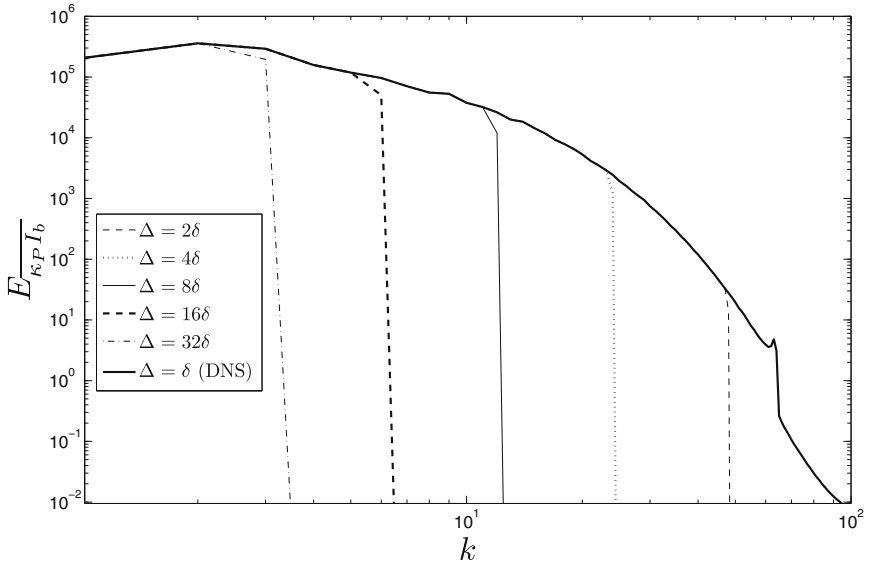

Fig. 3. Spectra of the filtered radiative emission term $\overline{\kappa_P I_b}$ for various filter sizes using the cut-off filter.

4. Results and discussion

4.1. Mean values of the SGS radiative emission and SGS radiative absorption terms

In LES of radiative heat transfer, there are two new terms that arise from the filtering operation applied to the RTE, and that require modelling. These are the SGS radiative emission $(\overline{\kappa_P I_b} - \bar{\kappa}_P \bar{I}_b)$ and the SGS radiative absorption $(\overline{\kappa_G I} - \bar{\kappa}_G \bar{I})$ terms. It is important to assess the relative importance of these terms compared to the resolved radiative emission $\bar{\kappa}_P \bar{I}_b$ and the resolved radiative absorption $\bar{\kappa}_G \bar{I}$ that are available at the LES grid points.

For this purpose we define two non-dimensional numbers,

$$R_{\kappa_P I_b} = \frac{\langle \overline{\kappa_P I_b} - \bar{\kappa}_P \bar{I}_b \rangle}{\langle \bar{\kappa}_P \bar{I}_b \rangle} \tag{27}$$

$$R_{\kappa_G I} = \frac{\langle \overline{\kappa_G I} - \bar{\kappa}_G \bar{I} \rangle}{\langle \bar{\kappa}_G \bar{I} \rangle} \tag{28}$$

where the brackets $\langle\ \rangle$ represent ensemble-average. Table 4 shows $R_{\kappa_P I_b}$ and $R_{\kappa_G I}$ for the standard conditions, whose physical parameters are listed in Table 3. The results were obtained using either a box or a cut-off filter, and several filter sizes. Important conclusions can be drawn from this table.

As expected, the SGS contain a relatively small fraction of the total radiative emission and absorption, *i.e.*, the most important values of radiative emission and absorption are associated with the resolved scales of motion. A similar situation is observed for

Table 4
Ratio of unresolved to resolved radiative emission and absorption terms – $R_{\kappa_P I_b}$ and $R_{\kappa_G I}$ – obtained from *a-priori* tests using box and cut-off filters and several filter sizes.

	Filter	$\Delta = 2\delta$	$\Delta = 4\delta$	$\Delta = 8\delta$	$\Delta = 16\delta$	$\Delta = 32\delta$
$R_{\kappa_P I_b}(\%)$	Box	0.205	0.920	2.87	6.56	11.6
$R_{\kappa_P I_b}(\%)$	Cut-off	9×10^{-5}	0.108	1.25	4.32	8.82
$R_{\kappa_G I}(\%)$	Box	0.00564	0.0276	0.101	0.377	1.03
$R_{\kappa_G I}(\%)$	Cut-off	9×10^{-5}	9×10^{-5}	0.00382	0.0781	0.534

many other important flow variables such as the velocity and temperature fields, and it is ultimately this fact that permits the modelling of turbulent flows using the LES technique. Recall from Ref. [22] that the filters $\Delta/\delta = 2$, 4 correspond to the dissipation range in the temperature spectra, and are therefore not interesting for LES, while the filters $\Delta/\delta = 8$ and 16 are near or at the inertial range region, which represents the ideal place for the implicit LES filter to be in classical SGS models. Finally, the filter $\Delta/\delta = 32$ is clearly placed in the energy containing scales of motion, which is too large for accurate LES for the velocity and temperature/scalar fields. Nevertheless, it is interesting to consider this filter here as it could be used in LES of radiative heat transfer in which one could choose a coarser grid than the LES grid used for the velocity and temperature/scalar fields, in order to reduce the computational cost of the radiative heat transfer computations.

Also, as expected, one can see that the relative importance of the SGS contribution to the total radiative emission and absorption terms increases with the filter size, and the SGS emission and absorption terms are higher for the box than for the cut-off filter. This last result is a well known fact observed in *a-priori* tests carried out on the momentum equations [31].

In the present work, we are interested in analyzing those features of the radiative heat transfer that are relevant for physical space, *i.e.*, LES using finite difference or finite volume codes, since this procedure is more often used in LES of turbulent flows for engineering applications. Therefore, in the remainder of this work, we will focus on the results obtained using the box filter, since this filter is implicitly associated with the discretization using central differences in finite volume codes [32].

Table 4 further shows that the SGS terms associated with the radiative absorption are much less important than the SGS terms associated with the emission. For instance, using a box filter with $\Delta/\delta = 32$, 11.6% of the emission and only about 1% of the absorption lie at the SGS. In agreement with this, the spectra of the (total) radiative emission and radiative absorption terms displayed in Fig. 4 show that, for high wave numbers, the emission term has more associated "energy" than the absorption term. This can be explained by the fact that the emission of radiation depends only on the local physical properties, whereas the absorption depends on the physical properties along the considered optical path. Consequently, the emission term is more sensitive to local fluctuations of the temperature. This fact suggests that in future LES models for the filtered RTE, more attention should be given to the modelling of the SGS emission terms, as they play a more important role in the evolution of the resolved thermal radiation.

4.2. Influence of the temperature turbulence intensity

The results from the previous section correspond to the standard case where the temperature turbulence intensity was set to $\sqrt{< T'^2 >}/< T > = 20\%$. However, in many reactive flows the turbulence intensity can reach much higher values, *e.g.*, it is not uncommon to find turbulence intensities of 30% or higher in flame jets [28]. Since an increase in the turbulence intensity is directly linked with an increase of the level of SGS energy in the flow (for a given grid size), it is important to assess the influence of this turbulent intensity on the ratio of SGS to resolved radiative emission and radiative absorption. To analyze this, Figs. 5(a) and (b) show values of $R_{\kappa_P I_b}$ and $R_{\kappa_G I}$, respectively, for several filter sizes and temperature turbulence intensities, using a box filter.

The temperature turbulence intensity has a strong influence on the mean SGS radiative emission and SGS radiative absorption, as shown by the increase of both $R_{\kappa_P I_b}$ and $R_{\kappa_G I}$ with $\sqrt{< T'^2 >}/< T >$. For instance, for $\Delta/\delta = 16$, an increase of $\sqrt{< T'^2 >}/< T >$ from 20% to 30% doubles the value of $R_{\kappa_P I_b}$ from 6% to 12%. For $\sqrt{< T'^2 >}/< T >= 30\%$ and $\Delta/\delta = 32$, $R_{\kappa_P I_b}$ reaches the extremely high value of 20%. Notice, however, that the relative importance of the SGS absorption terms is quite small in all cases. In the present results, $R_{\kappa_G I}$ is less than 2% even for the largest filter size $\Delta/\delta = 32$ and highest temperature turbulent intensity $\sqrt{< T'^2 >}/< T > = 30\%$, which again suggests that this term may be neglected in LES of radiative heat transfer. Therefore, we conclude that the effect of the temperature turbulence intensity is to increase (greatly) the relative importance of the unknown SGS terms in LES of radiative heat transfer.

4.3. Analysis of the Leonard, cross, and Reynolds SGS radiation terms

In classical LES based on the momentum equations, it is customary to decompose the filtered stresses tensor $\overline{u_i u_j}$ into the Leonard, cross and Reynolds SGS stresses. In the present work, we analyze the terms resulting from a similar decomposition applied to the filtered radiative emission $\overline{\kappa_P I_b}$ and to the filtered radiative absorption $\overline{\kappa_G I}$, as indicated in Eqs. (20) and (21). By applying the Reynolds averaging operator to these terms, and using a similar

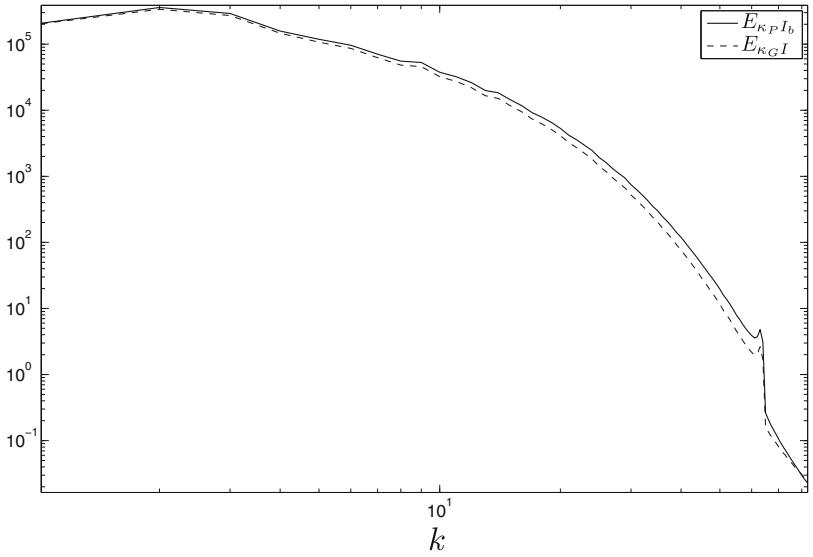

Fig. 4. Spectra of the (total) emission $\kappa_P I_b$ and absorption $\kappa_G I$ terms in the present isotropic turbulence data bank, for the standard conditions.

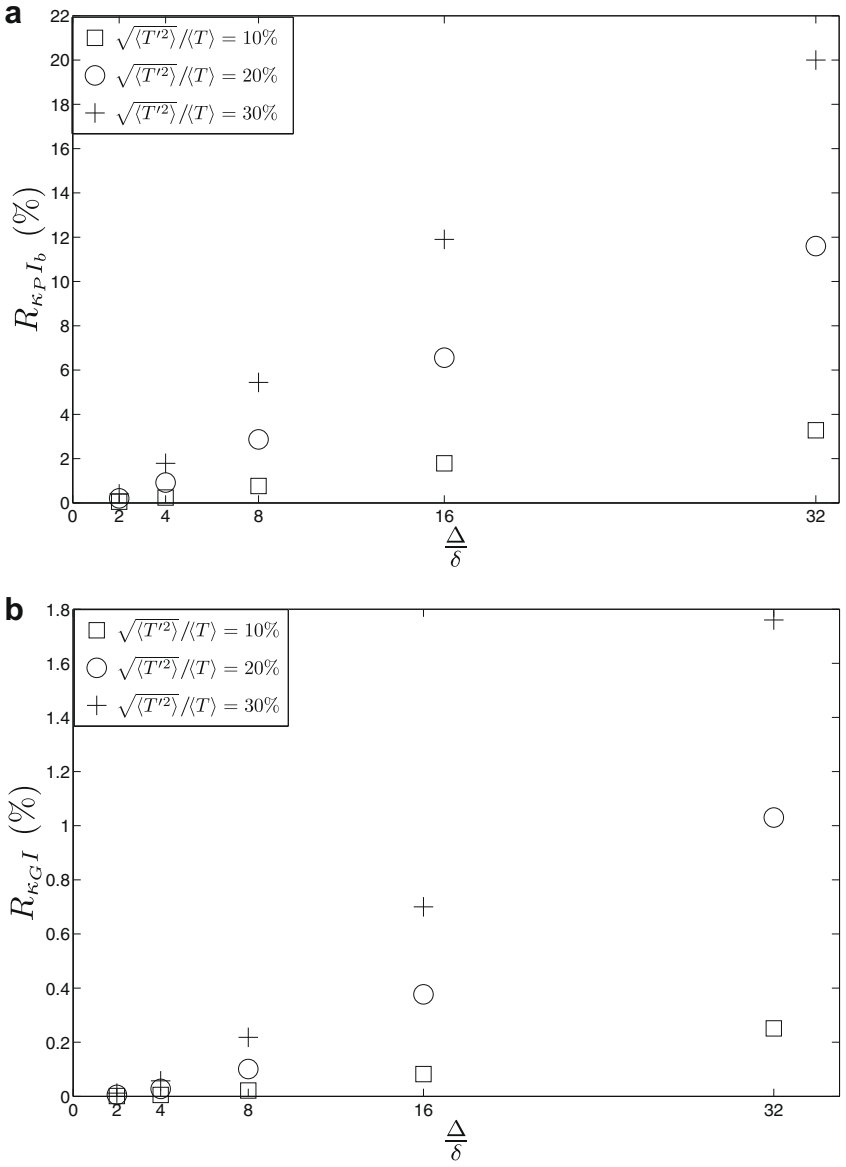

Fig. 5. Ratio of SGS to resolved emission and absorption ($R_{\kappa_P I_b}$ and $R_{\kappa_G I}$) for several filter sizes and temperature turbulence intensities (10%, 20% and 30%) using a box filter.

decomposition of the terms into Leonard, cross, and Reynolds terms, the following relations are obtained:

$$\langle\overline{\kappa_P I_b}\rangle = \langle\overline{\bar{\kappa}_P\bar{I}_b}\rangle + \langle\overline{\kappa''_P\bar{I}_b}\rangle + \langle\overline{\bar{\kappa}_P I''_b}\rangle + \langle\overline{\kappa''_P I''_b}\rangle \tag{29}$$

and

$$\langle\overline{\kappa_G I}\rangle = \langle\overline{\bar{\kappa}_G\bar{I}}\rangle + \langle\overline{\kappa''_G\bar{I}}\rangle + \langle\overline{\bar{\kappa}_G I''}\rangle + \langle\overline{\kappa''_G I''}\rangle \tag{30}$$

The Leonard terms, $\overline{\bar{\kappa}_P\bar{I}_b}$ and $\overline{\bar{\kappa}_G\bar{I}}$, represent the interactions between the resolved scales that contribute to $\overline{\kappa_P I_b}$ and $\overline{\kappa_G I}$, respectively, and therefore can be explicitly computed in LES. The cross terms $\overline{\kappa''_P\bar{I}_b} + \overline{\bar{\kappa}_P I''_b}$ and $\overline{\kappa''_G\bar{I}} + \overline{\bar{\kappa}_G I''}$ represent the interactions between the resolved and the unresolved terms, while the SGS Reynolds terms $\overline{\kappa''_P I''_b}$ and $\overline{\kappa''_G I''}$ represent the interactions between the unresolved quantities. Consequently, neither the cross nor the SGS Reynolds terms can be obtained from the resolved quantities, and need to be modelled in LES.

Tables 5 and 6 display the mean values of the SGS Leonard, cross, and Reynolds emission and absorption terms, normalized by $\langle\overline{\kappa_P I_b}\rangle$ and $\langle\overline{\kappa_G I}\rangle$, respectively, for several filter sizes using a box filter.

Table 5 shows that, in agreement with the previous results, at least concerning mean values, the contribution of the cross SGS radiative emission terms $\langle\overline{\kappa''_P\bar{I}_b} + \overline{\bar{\kappa}_P I''_b}\rangle$ and of the Reynolds SGS radiative emission terms $\langle\overline{\kappa''_P I''_b}\rangle$ for the filtered radiative emission $\langle\overline{\kappa_P I_b}\rangle$ is quite small. In particular, we see that $\langle\overline{\bar{\kappa}_P\bar{I}_b}\rangle \gg \langle\overline{\kappa''_P\bar{I}_b}\rangle + \langle\overline{\bar{\kappa}_P I''_b}\rangle + \langle\overline{\kappa''_P I''_b}\rangle$, *e.g.*, the sum of the cross and Reynolds SGS emission terms accounts for only about 7% of the total filtered emission $\langle\overline{\kappa_P I_b}\rangle$ for $\Delta/\delta = 16$. Notice that even when considering filter sizes characteristic of the energy-containing range, the sum of these

Table 5
Normalized mean values of the Leonard, cross and Reynolds SGS radiation emission terms for several filter sizes using a box filter.

	$\Delta = 2\delta$	$\Delta = 4\delta$	$\Delta = 8\delta$	$\Delta = 16\delta$	$\Delta = 32\delta$
$\langle\overline{\bar{\kappa}_P\bar{I}_b}\rangle/\langle\overline{\kappa_P I_b}\rangle$	1.00206	1.00929	1.0296	1.0702	1.131
$\langle\overline{\kappa''_P\bar{I}_b}\rangle/\langle\overline{\kappa_P I_b}\rangle$	-1.40×10^{-5}	−0.00342	−0.0111	−0.0209	−0.0290
$\langle\overline{\bar{\kappa}_P I''_b}\rangle/\langle\overline{\kappa_P I_b}\rangle$	-2.04×10^{-5}	−0.00344	−0.0111	−0.0209	−0.0291
$\langle\overline{\kappa''_P I''_b}\rangle/\langle\overline{\kappa_P I_b}\rangle$	−0.00202	−0.00243	−0.00733	−0.0284	−0.0734

Table 6
Normalized mean values of the Leonard, cross and Reynolds SGS radiation absorption terms for several filter sizes using a box filter.

	$\Delta = 2\delta$	$\Delta = 4\delta$	$\Delta = 8\delta$	$\Delta = 16\delta$	$\Delta = 32\delta$
$\langle\overline{\overline{\kappa_G}\overline{I}}\rangle/\langle\overline{\kappa_G I}\rangle$	1.0000564	1.000276	1.00110	1.00379	1.0104
$\langle\overline{\kappa''_G\overline{I}}\rangle/\langle\overline{\kappa_G I}\rangle$	-2.51×10^{-4}	-3.53×10^{-4}	-7.26×10^{-4}	−0.00179	−0.00367
$\langle\overline{\overline{\kappa_G}I''}\rangle/\langle\overline{\kappa_G I}\rangle$	-2.46×10^{-4}	-1.31×10^{-4}	-2.78×10^{-4}	−0.00143	−0.00345
$\langle\overline{\kappa''_G I''}\rangle/\langle\overline{\kappa_G I}\rangle$	-5.14×10^{-5}	-5.42×10^{-5}	-9.85×10^{-5}	-5.70×10^{-5}	−0.00327

terms reaches only about 13%. Table 5 shows also that for the larger filter sizes, which are important for LES, the SGS Reynolds emission term is slightly more important than the cross SGS radiative emission terms, although the relative importance of these terms is comparable. Therefore, future LES models developed to close the filtered radiative emission $\overline{\kappa_P I_b}$ have to take into account the influence of both the SGS cross and the SGS Reynolds emission terms.

Concerning the absorption, Table 6 confirms again that all the SGS terms contributing to the filtered radiative absorption are indeed very small, *e.g.*, the sum of the terms $\langle\overline{\kappa''_G\overline{I}}\rangle + \langle\overline{\overline{\kappa_G}I''}\rangle$ and $\langle\overline{\kappa''_G I''}\rangle$ accounts for only about 1% of the filtered radiative absorption $\overline{\kappa_G I}$ for the largest filter size $\Delta/\delta = 32$. Moreover, the cross and Reynolds terms display very similar magnitudes. This suggests that one may be tempted to neglect the influence of the SGS absorption in LES of radiative heat transfer.

However, one should be careful in generalizing conclusions. Since the instantaneous values of the flow quantities are used during the LES calculations, it is important to analyze how these averaged results translate into instantaneous data.

In order to analyze this issue, Figs. 6(a) and (b) present instantaneous profiles of the normalized SGS radiative emission and absorption terms, respectively, along a line of sight, which shows the type of fluctuations that may occur. The local coordinate along the line of sight was denoted by s (L is the size of the computational

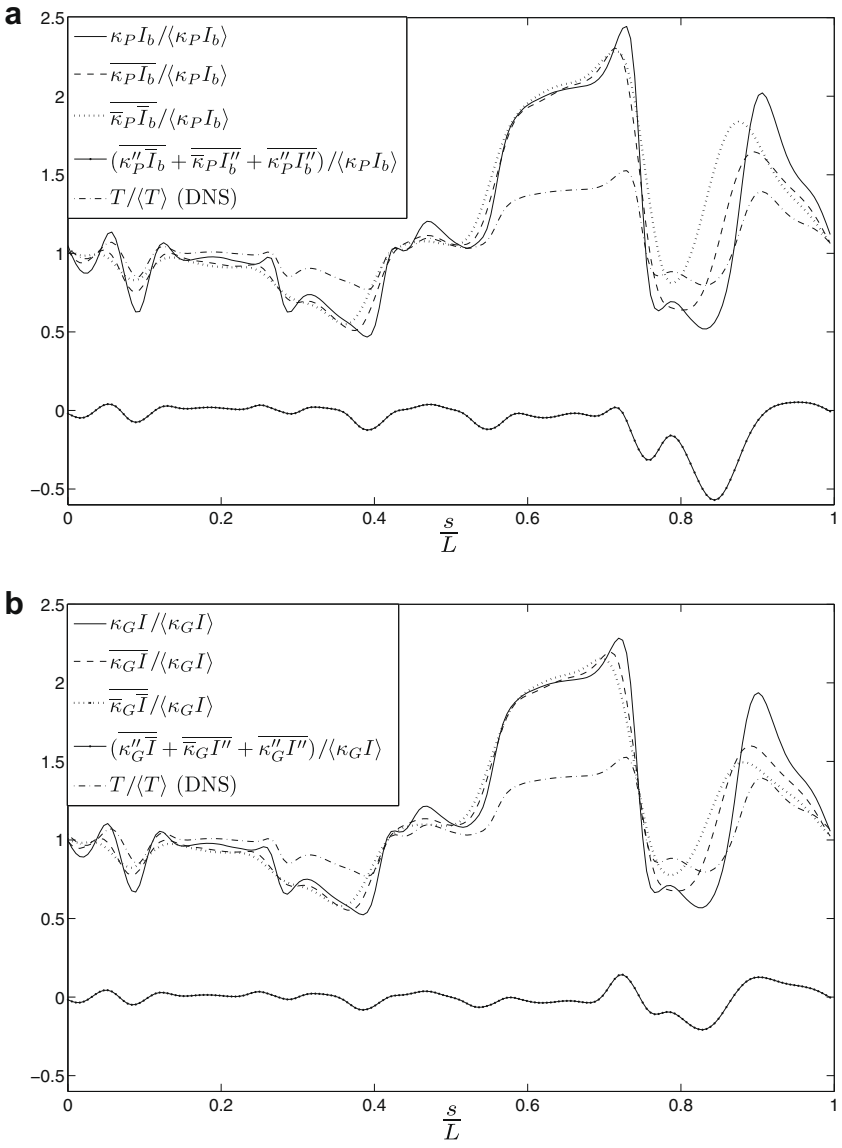

Fig. 6. Instantaneous profiles of the normalized SGS emission (a) and SGS absorption (b) terms along a line of sight, using a box filter with $\Delta = 8\delta$.

box), and a box filter of size $\Delta = 8\delta$ has been applied. As expected, the emission term is strongly correlated with the temperature. Moreover, the profiles of the emission and absorption terms in Figs. 6(a) and (b) are rather similar to each other, because the medium is in radiative equilibrium.

In this particular line of sight, the temperature has a maximum followed by a minimum between $0.7 < s/L < 0.9$. At about $s/L \approx 0.85$, the sum of the (normalized) SGS cross and SGS Reynolds radiative emission reaches about 50%. Clearly, the local influence of the unknown SGS terms is important at this location. Similarly, Fig. 6(b) shows that the sum of the SGS cross and SGS Reynolds radiative absorption terms becomes significant at some flow points, *e.g.*, the normalized sum for the SGS cross and SGS Reynolds radiative absorption attains a maximum of about 25%. However, we notice again that the influence of the SGS absorption terms is lower than that of the SGS emission. These observations have been verified for numerous other lines of sight chosen arbitrarily in the cubic domain.

To understand the behaviour of the SGS emission terms in the Fourier space, Figs. 7(a) and (b) show spectra of these terms using the box filter for $\Delta/\delta = 4$ and $\Delta/\delta = 16$, respectively. Notice that the wave number associated with these filter sizes is $k_c^{4\delta} = 24$ and $k_c^{16\delta} = 6$ [22], and the effect of the box filtering affects mainly wave numbers smaller than this implicit cut-off wave number. The spectrum of the (total) radiative emission $\kappa_P I_b$ is concentrated at the largest scales of motion $1 < k < 4$, and displays a fast decay after an inertial range region ($4 < k < 20$). Similar features are exhibited by the temperature/passive scalar spectrum [22]. The spectra from the filtered $\overline{\kappa_P I_b}$ and from the Leonard SGS radiative emission $\overline{\kappa_P}\overline{I_b}$ display similar trends. Naturally, for small wave numbers, the spectra from these quantities are virtually identical, *i.e.*, $E_{\kappa_P I_b} = E_{\overline{\kappa_P I_b}} = E_{\overline{\kappa_P} \overline{I_b}}$, and this low wave number range is smaller for $\Delta/\delta = 16$ than for $\Delta/\delta = 4$.

It is interesting to analyze the spectra from the cross and Reynolds SGS emission terms, $\overline{\kappa_P} I_b''$, $\overline{\kappa_P'' I_b}$, and $\overline{\kappa_P'' I_b''}$. Fig. 7(a) shows that for $\Delta/\delta = 4$, in agreement with the previous results, the SGS Reynolds emission term is much smaller than the two cross terms for the entire wave number range. In the case $\Delta/\delta = 16$, Fig. 7(b) shows a similar feature for most wave numbers, except at large wave numbers where the SGS Reynolds emission terms become more important than the cross terms. The most interesting observation displayed in these spectra concerns the peak wave number for the cross and Reynolds SGS emission terms. Indeed, all the spectra for these terms peak near the cut-off wave number, *e.g.*, for $\Delta/\delta = 16$, the cross SGS emission terms $\overline{\kappa_P} I_b''$ and $\overline{\kappa_P'' I_b}$ attain their

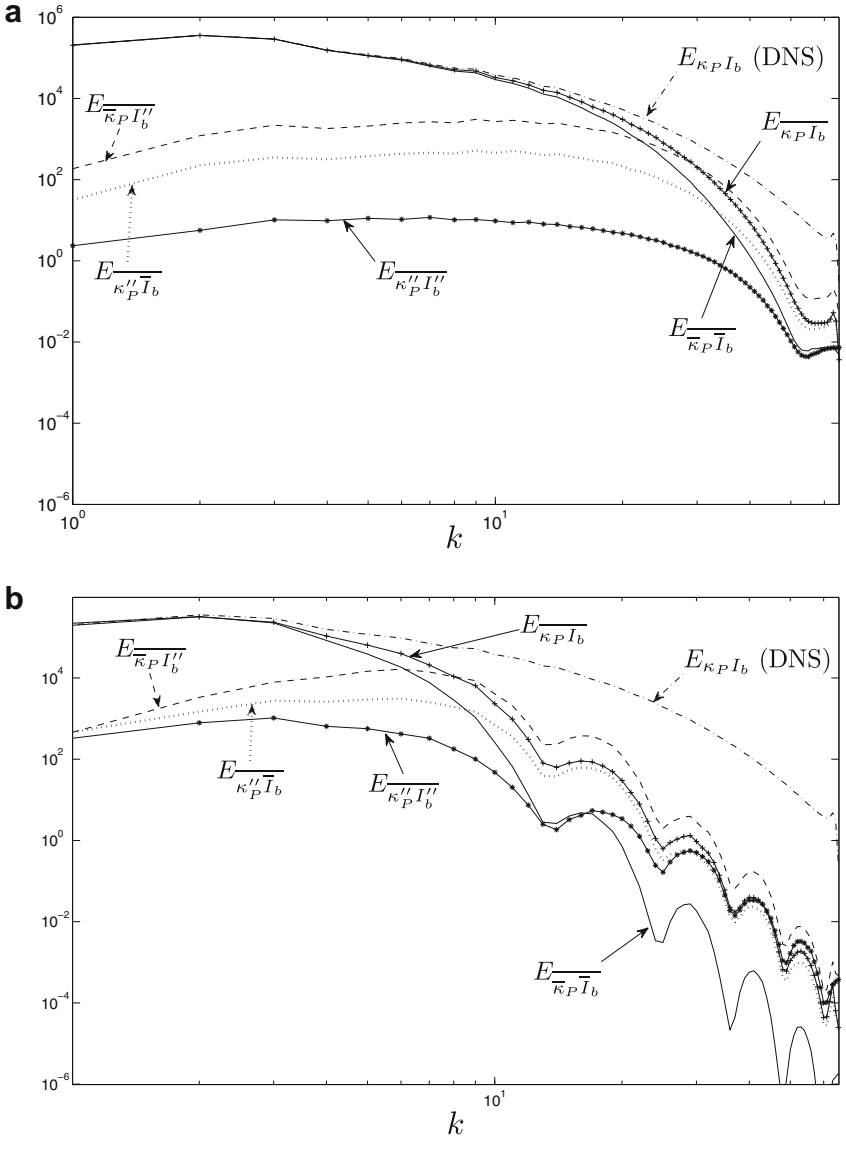

Fig. 7. Spectra of the SGS radiative emission terms for the box filter and for (a) $\Delta = 4\delta$ and (b) $\Delta = 16\delta$.

maximum at $k \approx 7$, which is near the cut-off wave number $k_c^{16\delta} = 6$. This suggests that any SGS model for these terms should be based on the filtered quantities obtained near the cut-off.

4.4. Discussion

The previous results showed that the SGS radiative emission is significantly higher than the SGS radiative absorption, and the SGS radiative absorption seems to contain only a very small fraction of the resolved radiative absorption. This suggests an assumption for the modelling of the SGS radiative absorption terms similar to the well-known optically-thin fluctuation approximation in Reynolds averaging, which states that the local spectral radiation intensity is weakly correlated to the local absorption coefficient: $\langle \kappa_\nu I_\nu \rangle \approx \langle \kappa_\nu \rangle \langle I_\nu \rangle$ [24]. According to this assumption, the filtered radiative absorption term can be approximated by the following relation:

$$\overline{\kappa_G I} \approx \bar{\kappa}_G \bar{I} \tag{31}$$

Analysis of the correlation coefficient between $\overline{\kappa_G I}$ and $\bar{\kappa}_G \bar{I}$ was undertaken for several filter sizes. It was observed that the correlation coefficient is quite insensitive to changes in filter size and is always greater than 99%, which further supports this approximation. This should be tested in *a-posteriori* tests, *i.e.*, in LES of radiative heat transfer, since, as shown before, local values of the SGS absorption terms may be significant. Notice, however, that the radiative absorption is a non-local term and therefore, if needed, a SGS model for this term could be particularly difficult to derive.

On the other hand, it has been shown that the SGS radiative emission terms must be modelled, particularly for LES in coarse meshes, as the ones commonly found in engineering applications and for flows with large temperature turbulent intensities. Since the SGS emission is dominated by local flow variables, it is plausible to assume that it can be modelled with a SGS model similar to the SGS models currently used to model the SGS scalar fluxes or the SGS stresses associated with LES of the temperature or velocity fields, respectively. Another approach consists in adapting to the LES context some models usually used for RANS simulation of the RTE [6]. For instance, the SGS radiative emission may be modelled by assuming a SGS probability density function, *e.g.*,

$$\overline{\kappa_P I_b}(\mathbf{r}, t) = \int_{T_{\min}}^{T_{\max}} \kappa_P(T) I_b(T) p(T, \mathbf{r}, t) dT \tag{32}$$

where $p(T, \mathbf{r}, t)$ is the SGS probability density function of the temperature in the case where the temperature is fully correlated with the species concentration. Similarly to the presumed PDF approach for TRI in RANS [8,33], a probability density function is introduced to model the effects of the SGS of the emission. This SGS probability density function approach has already been applied in LES modelling of combustion [34]. These aspects should be investigated in future works.

Another issue that deserves future investigation is soot radiation. It is well known that although the contribution of soot to thermal radiation is generally small in methane flames and moderate in propane flames, soot radiation often dominates over gas radiation in strongly sooting flames, *e.g.*, ethylene or acetylene flames. However, in contrast to temperature and species molar fractions, soot volumetric fraction cannot be expressed as a unique function of a passive scalar (*e.g.*, mixture fraction), using a state relationship. Therefore, the DNS code needs to be extended to compute soot volumetric fraction.

5. Conclusions

In the present work, *a-priori* tests were carried out in order to investigate the relative importance of the unknown SGS terms arising from the spatial filtering operation applied to the radiative transfer equation, and that have to be modelled in LES involving important radiation effects. The unknown unclosed terms of the filtered radiative source term are the SGS radiative emission $(\overline{\kappa_P I_b} - \bar{\kappa}_P \bar{I}_b)$ and the SGS radiative absorption $(\overline{\kappa_G I} - \bar{\kappa}_G \bar{I})$, and represent the effect of the SGS radiation on the evolution of the resolved divergence of the radiative source term.

The study used classical *a-priori* tests to extract the exact terms involved in LES of RTE through a spatial filtering operation applied to fields originated in a DNS of isotropic turbulence. Instantaneous fields of temperature and species concentration from the DNS were rescaled to represent data from the far field of a turbulent jet downstream of the flame front. A ray-tracing method was used to solve the RTE along lines of sight in the DNS grid.

The analysis of their spectra has shown that the most important values of both the SGS radiative emission and the SGS radiative absorption are concentrated at the large scales of motion. This makes the LES approach feasible for radiative heat transfer computations. Moreover, these terms can be decomposed into Leonard, cross, and SGS Reynolds terms, which are similar to the terms derived from the filtered momentum equations. The SGS cross and SGS Reynolds terms, which are much smaller than the Leonard terms, display similar orders of magnitude. Their spectra show that they peak near the implicit cut-off filter, which indicates that any SGS model for these terms must be defined in terms of quantities dominated by scales of motion near the implicit LES filter.

Using a box filter, which corresponds to the discretization procedures most frequently used in engineering applications, the mean SGS radiative emission and the mean SGS radiative absorption represent about 7% and 0.4%, respectively, of the mean resolved radiative emission and radiative absorption for a temperature turbulence intensity of 20% and a filter size characteristic of the inertial range region of the temperature field ($\Delta/\delta = 16$). Notice however that the local and instantaneous values of these terms can be substantially higher, which means that the local "dynamics" of the RTE will be even more affected by these terms. Thus, the magnitude of the SGS radiative emission term is similar to the magnitude of the SGS stresses from the momentum equations, whereas the SGS radiative absorption terms revealed to be much smaller. This result suggests that in many applications, the SGS radiative absorption terms may be neglected, *i.e.*, these terms may be modelled by simply assuming $\overline{\kappa_G I} \approx \bar{\kappa}_G \bar{I}$.

The effects of the filter type, filter size and temperature turbulence intensity were studied in the SGS radiative emission and SGS radiative absorption terms. Using a cut-off filter, the SGS terms tend to be smaller than when using a box filter, but the trends with the filter size and temperature turbulence intensity are the same: both the SGS radiative emission and SGS radiative absorption increase substantially with the filter size and temperature turbulence intensity. Thus, the relative importance of the SGS unknown terms in LES of radiative heat transfer increases for LES in coarser meshes, as the ones currently used in engineering applications, and for flows with high turbulence intensity, such as jets and wakes, which are often encountered in combustion devices. This makes the modelling of these terms very important in LES of radiation. This topic should be addressed in future works.

Acknowledgements

This work was developed within the framework of Project PPCDT/EME/59879/2004, which is financially supported by FCT-Fundação para a Ciência e a Tecnologia, Project No. 3599. M. Roger acknowledges the FCT-Fundação para a Ciência e a Tecnologia for the post-doc fellowship SFRH/BPD/34014/2006.

References

[1] S.B. Pope, Turbulent Flows, Cambridge University Press, Cambridge, 2000.
[2] J. Janicka, A. Sadiki, Large eddy simulation of turbulent combustion systems, Proc. Combust. Inst. 30 (1) (2005) 537–547.
[3] H. Pitsch, Large-eddy simulation of turbulent combustion, Annu. Rev. Fluid Mech. 38 (2006) 453–482.
[4] D. Veynante, D.L. Vervish, Turbulent combustion modeling, Prog. Energy Combust. Sci. 28 (3) (2002) 193–266.
[5] K. Mahesh, G. Constantinescu, P. Moin, A numerical method for large-eddy simulation in complex geometries, J. Comput. Phys. 197 (1) (2004) 215–240.
[6] P.J. Coelho, Numerical simulation of the interaction between turbulence and radiation in reactive flows, Prog. Energy Combust. Sci. 33 (4) (2007) 311–383.
[7] S.P. Burns, Turbulence radiation interaction modeling in hydrocarbon pool fire simulations, Report No. SAND99-3190, Sandia National Laboratories, 1999.
[8] P.J. Coelho, O.J. Teerling, D. Roekaerts, Spectral radiative effects and turbulence–radiation interaction in a nonluminous turbulent jet diffusion flame, Combust. Flame 133 (1–2) (2003) 75–91.
[9] P.J. Coelho, Detailed numerical simulation of radiative transfer in a nonluminous turbulent jet diffusion flame, Combust. Flame 136 (4) (2004) 481–492.
[10] L. Tessé, F. Dupoirieux, J. Taine, Monte Carlo modeling of radiative transfer in a turbulent sooty flame, Int. J. Heat Mass Transfer 47 (3) (2004) 555–572.
[11] S. Mazumder, M.F. Modest, A probability density function approach to modeling turbulence–radiation interactions in nonluminous flames, Int. J. Heat Mass Transfer 42 (6) (1999) 971–999.
[12] G. Li, M.F. Modest, Application of composition pdf methods in the investigation of turbulence–radiation interactions, J. Quant. Spectrosc. Radiat. Transfer 73 (2–5) (2002) 461–472.
[13] A. Wang, M.F. Modest, D.C. Haworth, L. Wang, Monte Carlo simulation of radiative heat transfer and turbulence interactions in methane/air jet flames, J. Quant. Spectrosc. Radiat. Transfer 109 (2) (2008) 269–279.
[14] Y. Wu, D.C. Haworth, M.F. Modest, B. Cuenot, Direct numerical simulation of turbulence/radiation interaction in premixed combustion systems, Proc. Combust. Inst. 30 (1) (2005) 639–646.
[15] K.V. Deshmukh, D.C. Haworth, M.F. Modest, Direct numerical simulation of turbulence–radiation interactions in homogeneous nonpremixed combustion systems, Proc. Combust. Inst. 31 (1) (2007) 1641–1648.
[16] P.E. Desjardin, S.H. Frankel, Two-dimensional large eddy simulation of soot formation in the near-field of a strongly radiating non-premixed acetylene–air turbulent jet flame, Combust. Flame 119 (1–2) (1999) 121–132.
[17] D.C Haworth, V. Singh, A. Gupta, M.F. Modest, Large eddy simulation of turbulent flows with thermal radiation and turbulence/radiation interaction, 58th Annual Meeting of the American Physical Society Division of Fluid Dynamics, 2005.
[18] W.P. Jones, M.C. Paul, Combination of DOM with LES in a gas turbine combustor, Int. J. Eng. Sci. 43 (5–6) (2005) 379–397.
[19] R. Gonçalves dos Santos, M. Lecanu, S. Ducruix, O. Gicquel, E. Iacona, D. Veynante, Coupled large eddy simulations of turbulent combustion and radiative heat transfer, Combust. Flame 152 (3) (2008) 387–400.
[20] D. Poitou, M. El Hafi, B. Cuenot, Diagnosis of turbulence–radiation interaction in turbulent flames and implications for modeling in large eddy simulation, Turkish J. Eng. Environ. Sci. 31 (6) (2007) 371–381.
[21] M. Roger, P.J. Coelho, C.B. da Silva, Analysis of the relevance of the filtered radiative transfer equation terms for large eddy simulation of turbulence–radiation interaction, Proc. CHT-08 ICHMT Int. Symp. Adv. Comput. Heat Transfer, Marrakech, Morocco, 2008.
[22] C.B. da Silva, J.C.F. Pereira, Analysis of the gradient-diffusion hypothesis in large-eddy simulations based on transport equations, Phys. Fluids 19 (035106) (2007).
[23] J. Smagorinsky, General circulation experiments with the primitive equations, Mon. Weather Rev. 91 (3) (1963) 99–164.
[24] M.F. Modest, Radiative Heat Transfer, McGraw-Hill, New York, 2003.
[25] C.B. da Silva, J.C.F. Pereira, On the local equilibrium of the subgrid-scales: the velocity and scalar fields, Phys. Fluids 17 (108103) (2005).
[26] K. Alvelius, Random forcing of three-dimensional homogeneous turbulence, Phys. Fluids 11 (7) (1999) 1880–1889.
[27] C.B. da Silva, I. Malico, P.J. Coelho, J.C.F. Pereira, An exploratory investigation of radiation in homogeneous isotropic turbulence, in: Proc. Eurotherm 78 – Comput. Thermal Radiation in Participating Media II, Poitiers, France, 2006, pp. 215–224.
[28] http://public.ca.sandia.gov/TNF/simplejet.html.
[29] R.M. Goody, R. West, L. Chen, D. Crisp, The correlated-*k* method for radiation calculations in non-homogeneous atmospheres, J. Quant. Spectrosc. Radiat. Transfer 42 (6) (1989) 539–550.
[30] A. Soufiani, J. Taine, High temperature gas radiative property parameters of statistical narrow band model for H_2O, CO_2, and CO, and correlated-*K* model for H_2O and CO_2, Int. J. Heat Mass Transfer 40 (4) (1997) 987–991.
[31] U. Piomelli, Y. Yunfang, R. Adrian, Subgrid-scale energy transfer and near-wall turbulence structure, Phys. Fluids 8 (1) (1996) 215–224.
[32] R. Rogallo, P. Moin, Numerical simulation of turbulent flows, Annu. Rev. Fluid Mech. 16 (1984) 99–137.
[33] L.H. Liu, X. Xu, Y.L. Chen, On the shapes of the presumed probability density function for the modeling of turbulence–radiation interactions, J. Quant. Spectrosc. Radiat. Transfer 87 (3–4) (2004) 311–323.
[34] T. Poinsot, D. Veynante, Theoretical and Numerical Combustion, Edward Inc., 2001.